Statistical performance evaluation of electrostatic micro actuators for a deformable mirror

Raji Krishnamoorthy, Thomas Bifano, Guido Sandri

Department of Aerospace and Mechanical Engineering
110 Cummington Street
Boston University, Boston MA 02215

ABSTRACT

This paper describes a study to characterize the performance of surface micromachined electrostatic actuators, with a brief introduction to some MEMS (microelectromechanical systems) mirrors developed at BU incorporating these actuators. Fixed-fixed actuators were extensively tested to determine suitability for optical applications, and specifically for an adaptive optics imagining system. The critical issues relating to device performance, namely yield (indicating robustness and process reliability), position repeatability, precision and frequency response, were quantified in the research effort described here. The study demonstrated 95% device yield, 10 nm position repeatability (99% confidence levels), and greater than 66 kHz frequency bandwidth.

KEYWORDS : Deformable mirrors, MEMS, electrostatic actuators, characterization, repeatability

2. INTRODUCTION

A new class of silicon-based deformable mirror for use in adaptive optics and other optical applications is being developed[1]. The mirror is supported on an array of electrostatically-controlled microactuators that can be coordinated to achieve precise actuation and control at a macroscopic level. Several types of actuators as well as parallel arrays of actuators with segmented and continuous mirrors have been designed, fabricated and tested. Fig. 1 is a schematic of the cross-section through a three-element continuous mirror, with the central actuator deflected. The continuous mirror is actuated at discrete points, the deformation being normal to the surface and continuous over the actuation range. The actuators are fixed-fixed beams and the mirror is attached to each actuator at midspan by a post. When voltage is applied between an actuator and the substrate or an address pad, the electrostatic force developed deflects the actuator toward the substrate. The targeted applications for this MEMS deformable mirror include adaptive optical imaging and projection systems, and optical correlators for pattern recognition systems. The motivation for a detailed study and statistical analysis of actuator behavior stems from the requirements for high repeatability and resolution in these applications.

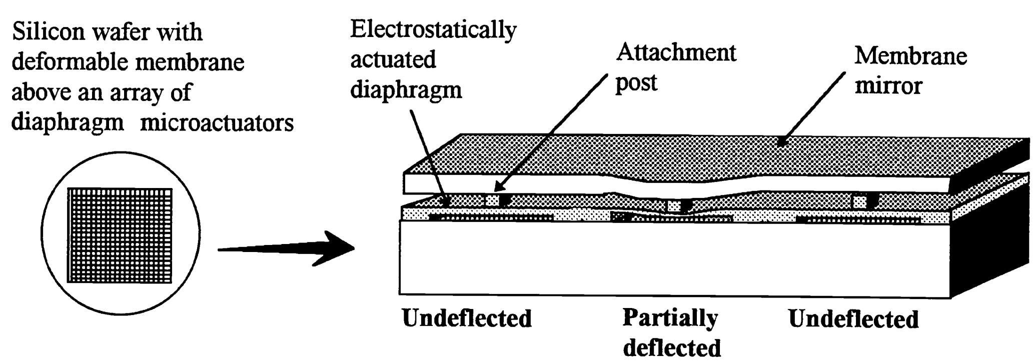

Figure 1: Schematic cross-section of a section of deformable mirror array showing actuator deflection

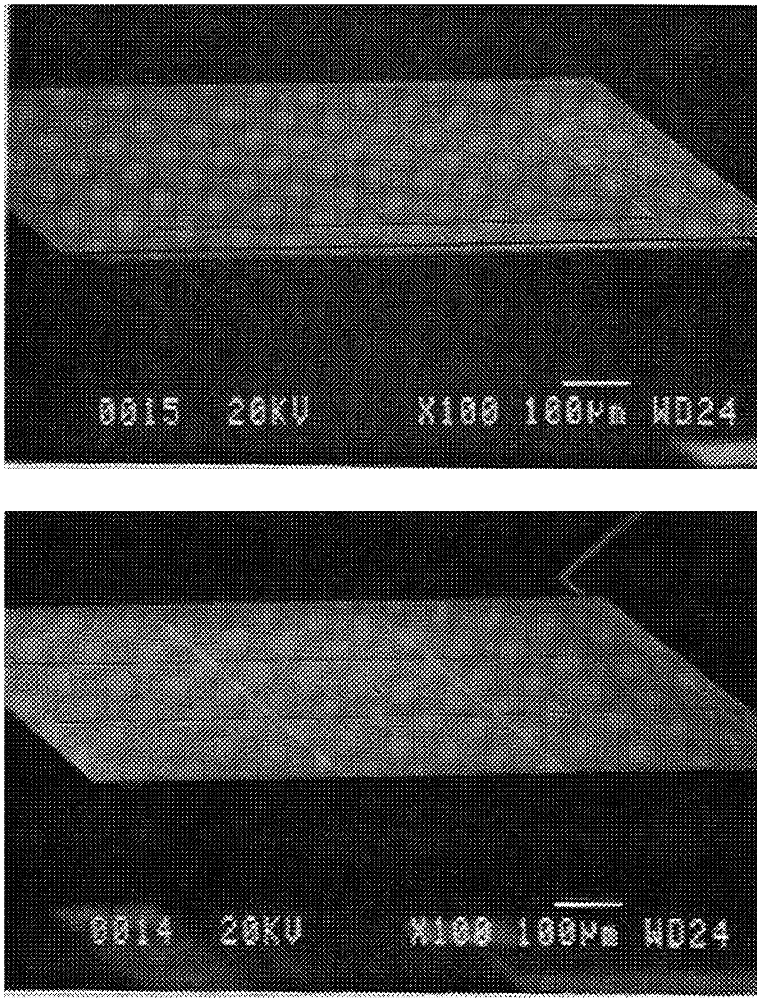

Figure 2: SEM photographs of nine element continuous (top) and segmented (bottom) mirror arrays

Fig. 2 shows scanning electron micrographs of nine element (3x3) continuous and segmented mirrors. The fixed-fixed actuators in these arrays are 200 μm square with the attachment posts being 250μm apart. The fill-factor of the segmented mirror array in this design is 92%.

A 16 element segmented mirror array was wire bonded to a standard package (a 64 pin DIP), from which connections were made to a control interface. Fig. 3 shows a photograph of the mirror array wire bonded to a chip carrier and mounted on a PC board. A twenty channel control circuit has been built, addressed through software, and used for high speed control of this segmented mirror array. The fill-factor of this segmented mirror is very low (32%), and it was primarily used for testing the control interface and circuitry.

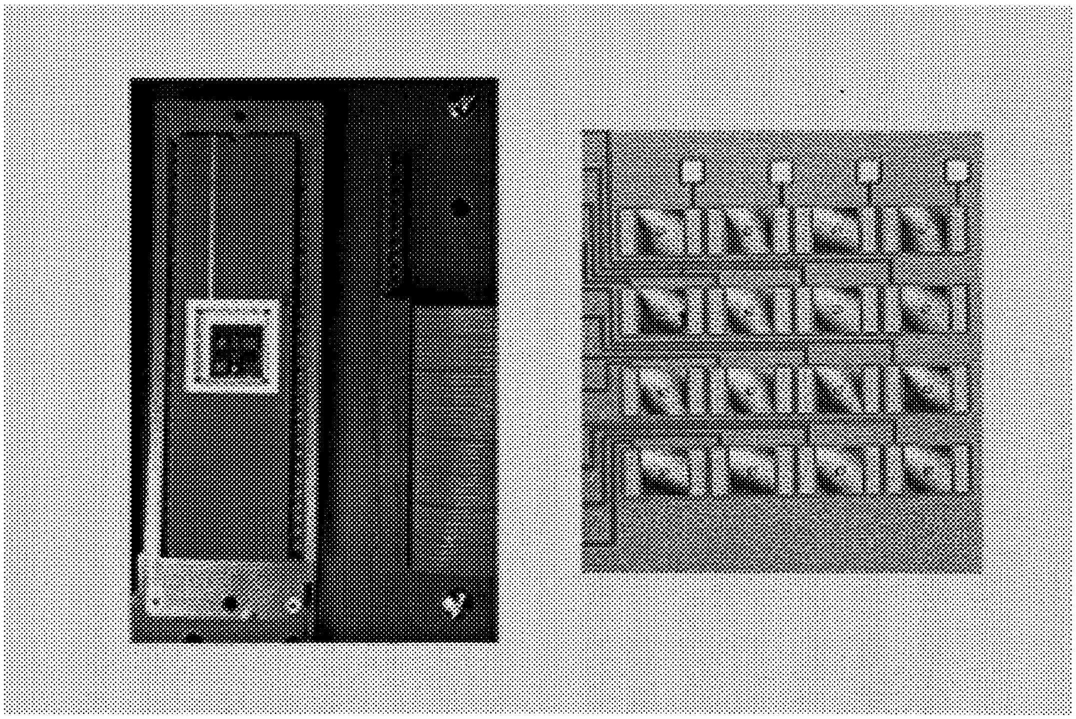

Figure 3 : Photograph of wafer wire bonded to a standard 64 pin chip carrier (left) and optical micrograph of 16 element segmented mirror array (right).

3. DESIGN AND FABRICATION

All test devices were fabricated using MUMPs[2], a three-layer polycrystalline silicon surface-micromachining process. Figure 4 shows a cross-sectional schematic view of a micromachined actuator with a portion of a mirror sheet over it. The first polysilicon layer is used for address pads and the others for the actuators and mirror respectively. Holes are patterned into the top two polysilicon layers to enable subsequent release by wet chemical etch of the sacrificial oxide layers.

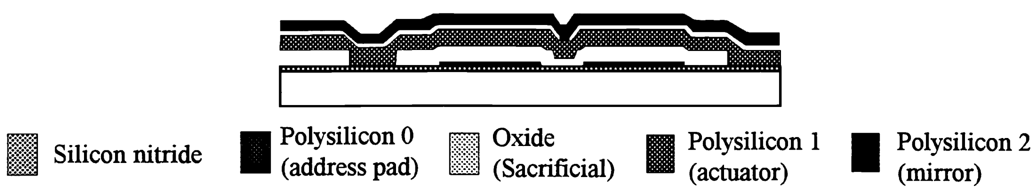

Figure 4 : Schematic of fabricated deformable mirror test structure using MUMPs

Fixed-fixed actuators were chosen since they are structurally simple, yet robust. Since devices were fabricated in a foundry process, layer thicknesses were fixed, and test devices had 2 μm gap and 3.5 μm thickness. Lateral dimensions were chosen to be 350 μm x 350 μm for these actuators based on design criteria for keeping actuation voltage low and simultaneously avoiding buckling due to residual stress. This optimum design was chosen based on theoretical and numerical calculations, as well as experimental results from previous MUMPs runs, where several actuator geometries and shapes were fabricated and tested. Figure 5 is a schematic of the described individual actuator used for all the tests described in this paper.

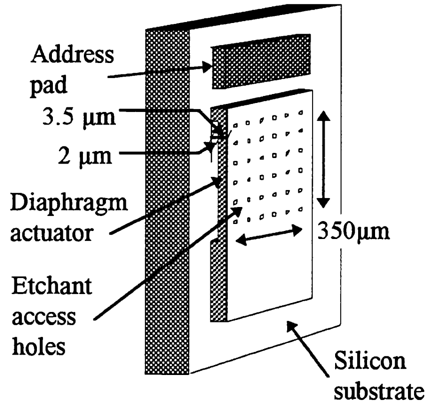

Figure 5 : Schematic of an individual test actuator, showing optimum dimensions.

Previous MEMS research demonstrated that the average yield for individual micro-sensors and micro-actuators is 40-60%. Massively parallel, multiple micro-actuator systems implementing macroscopic function require higher yields (greater than 90%) and designs with fault-tolerant function. Device yield is therefore a major concern, and experiments to characterize this have given optimistic results. A total of 487 individual actuators were tested in one study, with a yield of 94.5% useful, working actuators.

4. INTERFEROMETRIC MEASUREMENT SETUP

The wafer containing the devices was mounted on a three axis stage. Voltage was applied to the device using standard tungsten micro-probes, and deflection was measured at the center of the device. The driving signal was generated by a software controlled digital-to-analog integrated circuit, and followed by a high-performance voltage amplifier with 100 kHz bandwidth.

Deflections were measured using the Zygo ZMI 1000 system - a single point, split frequency displacement measuring laser interferometer. This device uses a focused laser beam to measure normal displacement with a position resolution of 2.5 nm and time resolution of 15.6 ns, a range of $\pm$ 250 µm about focus, a frequency bandwidth of 0-133 kHz, and a lateral averaging area of several micrometers.

The incoming laser beam has two components that are orthogonally polarized and 20 MHz apart in frequency. This beam is divided by the polarization beamsplitter into the two orthogonally polarized components (Fig. 6). The reference beam passes through the quarter waveplate and is reflected back from the retroreflector. The measurement beam passes through a quarter waveplate and is focused on the measurement surface. Displacement of the measurement surface causes a change in the optical path difference of the two beams. When they recombine at the beamsplitter, the polarization of both beams has been rotated by 90 degrees, causing them to enter the photodetector and isolating the laser. The interference of the recombined beams is converted into an electrical signal by the receiver.

The experimental setup was placed on a vibration-free air table, located in an area where temperature was not accurately controlled. Under these conditions, the dead path error (difference in distance in air between the reference and measurement paths when the interferometric error is initiated or zeroed) was about 20 nm. This dead path error occurs due to environmental changes (temperature, air pressure and humidity) during the measurement. A differential interferometer was designed and built (Fig. 6), to balance the optical paths and reduce these effects over the course of a measurement. Some performance improvement was observed with this optical configuration, and error motion was reduced to ~ 15 nm.

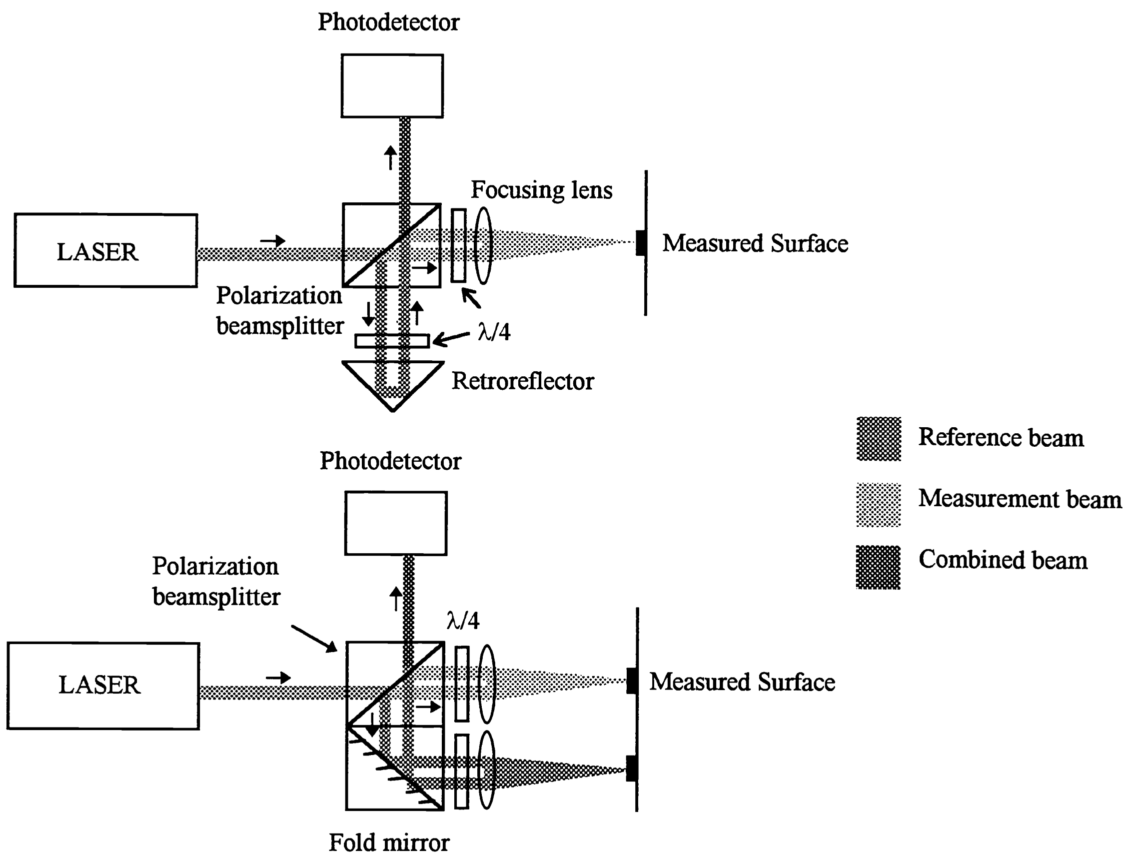

Figure 6 : Laser interferometer system used for device characterization. Top: Single-path optical configuration of interferometer. Bottom: Differential interferometer developed to reduce noise. Motion resolution is 2.5 nm and measurement bandwidth is 133 kHz.

To decrease noise floor, the space was enclosed and all equipment that might interfere with the measurement, including ventilating blowers, were turned off. The noise floor then reduced to the motion resolution of the interferometer (2.5 nm) for the duration of the test. Under these environmental conditions, both optical configurations yielded the same performance. All the measurements for the repeatability study were made under these circumstances.

A customized windows-based software interface for the interferometer was developed using Borland C++. Data can be plotted real time for low sample rates (< 25 Hz). The software can be customized to provide user-controlled actuation voltage signals, depending on the experimental requirement. The output from such an actuation signal can then be visualized and analyzed.

5. MEASURED ACTUATOR RESPONSE

Fig. 7 shows the typical response of the test actuator to a voltage ramp. The actuator membrane deflected nonlinearly with increasing voltage as shown by the solid line. At the critical or pull-in voltage, it snapped down to the substrate. When voltage was decreased, the membrane remained in its snapped position until some voltage lower than the pull-in voltage, when it decreased nonlinearly following the path along which it had increased. For this test device, the pull-in voltage was measured to be 60V and the release voltage was 50V.

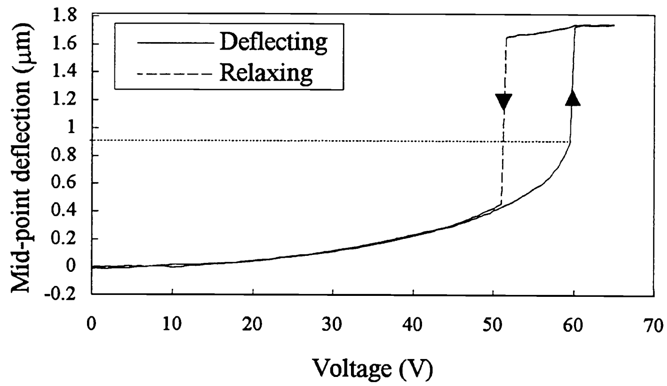

Figure 7 : Measured deflection as a function of increasing and decreasing voltage

For open-loop actuator control, the pull-in and hysteresis are undesirable phenomena. The operating range is therefore restricted by the pull-in voltage. When subjected to a voltage ramp (0-50V), the test actuator's membrane deflected non-linearly, but reversibly, by 0.5 μm, as shown in Figure 8.

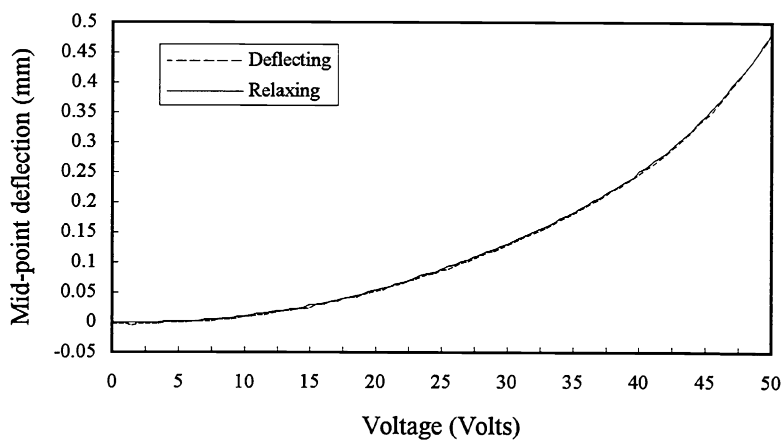

Figure 8 : Measured deflection as a function of increasing and decreasing voltage

The actuators drew no measurable current, which implies that the array is thermodynamically reversible, as expected for an electrostatic system. There was no electrical coupling between actuators.

6. POSITION REPEATABILITY

Position repeatability was measured for several actuators through ensemble averaging of the data from a series of ramp actuation tests. A typical data set consisted of 100 sample runs to produce an ensemble of records of deflection as a function of voltage. Experimental conditions were kept as statistically similar as possible over the course of acquiring a set of data. The applied voltage was in the form of a ramp from 0-50 V with deflection data measured at 0.5 V increments, followed by a 50-0 V ramp. Since there was no hysteresis observed, displacement data corresponding to the ramp up and the ramp down was treated as identical, resulting in 200 sample data points at each voltage value. The data was analyzed using standard statistical analysis procedures for random data[3].

Results are presented for an ensemble of 200 records, with measurement resolution of 200 nm. Fig. 9 shows the ensemble averaged displacement curve with the sigma-limits corresponding to 99% probability.

The limits were calculated based the normal curve, using the unbiased ensemble mean and standard deviation estimates. For example,

$$\mathrm{P}(\bar{\mu} - 2.58\bar{\sigma} < y \le \bar{\mu} + 2.58\bar{\sigma}) = 99\% \tag{1}$$

where the unbiased estimates of mean and variance were calculated as :

$$\bar{\mu}_y(V) = \frac{1}{N}\sum_{i=1}^{N} y_i(V) \tag{2}$$

$$\bar{\sigma}_y^2(V) = \frac{1}{N-1}\sum_{i=1}^{N} [y_i(V) - \bar{\mu}_y(V)]^2 \tag{3}$$

The average standard deviation along the curve is 1.89 nm, resulting in an average position repeatability of 9.76 nm (for 99% confidence levels).

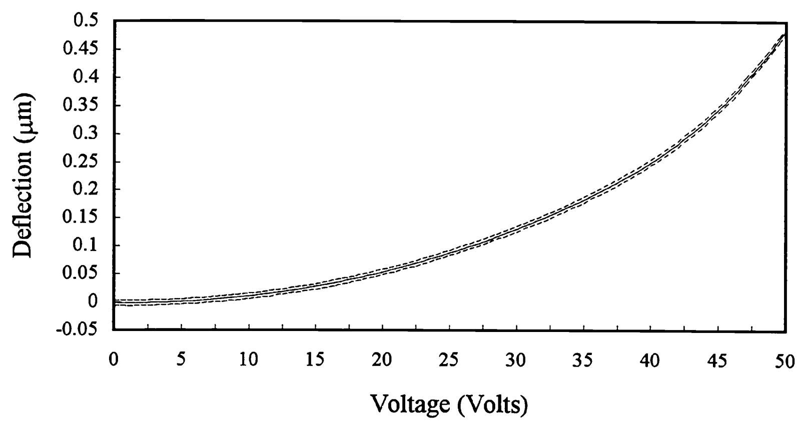

Figure 9 : Position repeatability of actuator (ensemble averaged mean curve with limits corresponding to 99% probability)

Confidence intervals for the mean value $\mu_y(V)$ have been constructed based on the estimates of mean and variation, $\bar{\mu}_y(V)$ and $\bar{\sigma}_y^2(V)$. The (1 - α) confidence interval at any voltage V is

$$\bar{\mu}_y(V) - \frac{\bar{\sigma}_y(V) t_{n;\alpha/2}}{\sqrt{N}} \le \mu_y(V) < \bar{\mu}_y(V) + \frac{\bar{\sigma}_y(V) t_{n;\alpha/2}}{\sqrt{N}} \tag{4}$$

where $\bar{\sigma}_y(V) = \sqrt{\bar{\sigma}_y^2(V)}$ is an unbiased estimate of the standard deviation of $y(V)$ at voltage V, and $t_{n;\alpha/2}$ is the $\alpha/2$ percentage point of Student's t variable with $n = N - 1$ degrees of freedom. This construction for the confidence interval applies even if $y(V)$ is not normally distributed, as long as the sample size is large ($N > 50$), such as the one under consideration. Figure 10 shows the 99% confidence intervals on mean displacement as a function of voltage, for 200 repeated actuations of a single actuator.

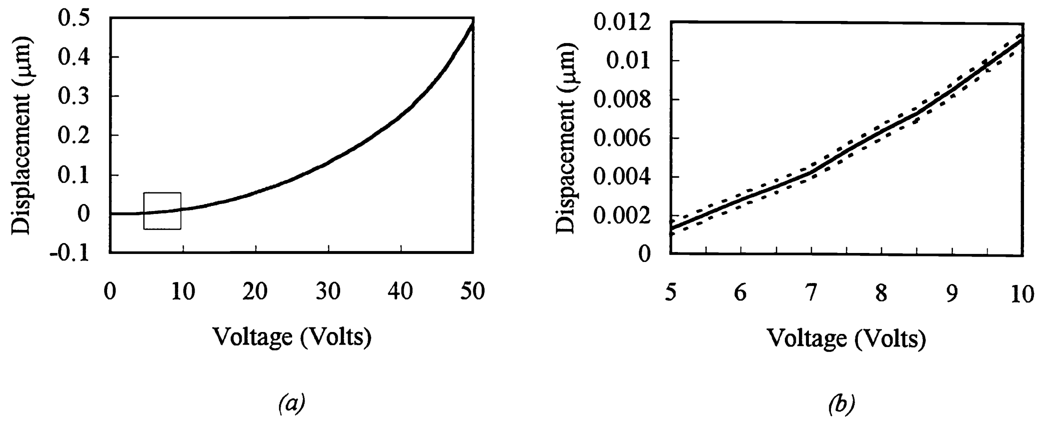

Figure 10 : (a) Sample mean with 99% confidence intervals on the deflection of a single actuator. Average interval = 0.0006μm. (b) Inset showing the curves in the 5-10V range

Confidence intervals for the variance have been evaluated as

$$\frac{n\bar{\sigma}_y^2(V)}{\chi^2_{n;\alpha/2}} \leq \sigma_y^2(V) < \frac{n\bar{\sigma}_y^2(V)}{\chi^2_{n;1-\alpha/2}} \tag{5}$$

where χ^2_n is the chi-square variable with $n = N - 1$ degrees of freedom. Figure 11 shows the ensemble variance estimate with 99% confidence intervals.

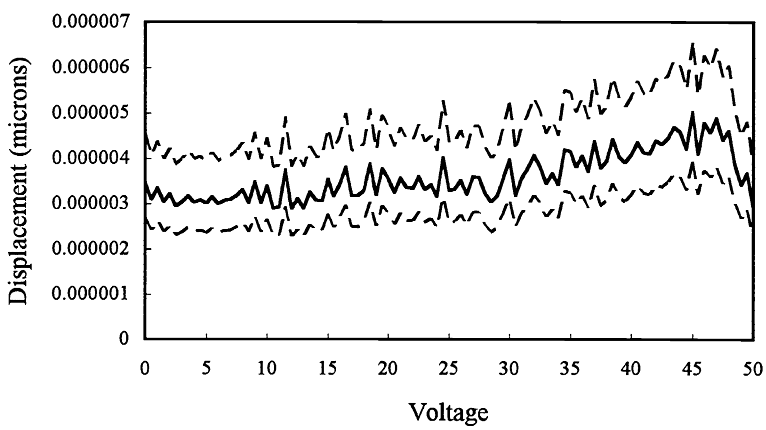

Figure 11 : Ensemble variance with 99% confidence intervals

The chi-square (χ^2)goodness-of-fit test was used to test the equivalence of the probability density function of the sample data to the normal distribution[4]. The χ^2 test requires the data to be divided into bins with at least 5 samples in each bin. This generates the observed distribution, which is compared with the expected Gaussian distribution using the computed value of χ^2 as the acceptance criterion. Figure 12 shows the distribution at 30 V for the data analyzed above, with a Gaussian fitted to it. The underlying physical process is continuous, but sampling is discrete, and the quantization of the sampled data is obvious in the figure; the data could not be subjected to a χ^2 test since it did not meet the minimum criteria for number of bins/number of samples per bin.

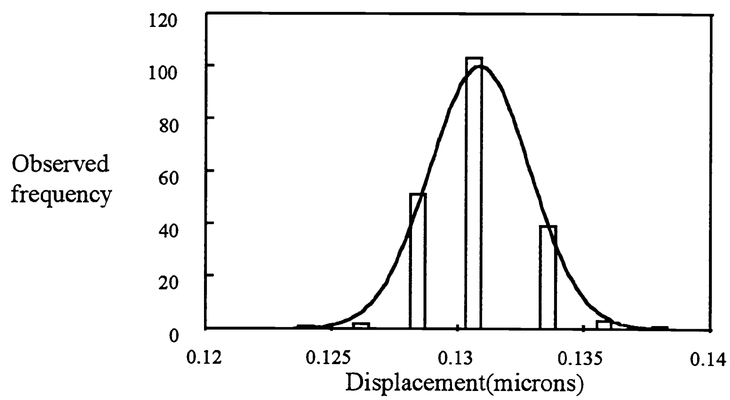

Figure 12 : Observed frequency distribution and normalized Gaussian

The χ^2 test was applied to another set of data from the same experimental setup, but with greater dispersion (caused by environmental noise). The average standard deviation in this case was 20 nm. Figure 13 shows the distribution and corresponding Gaussian for this data. The null hypothesis was found to be true in this case. This suggests that the former data is also normally distributed.

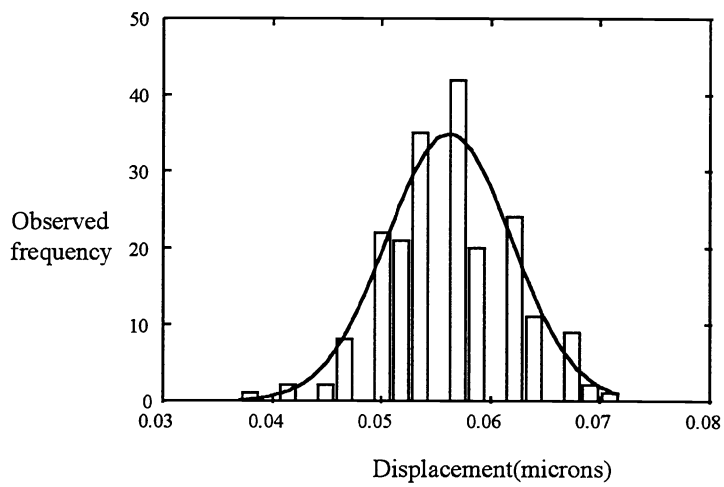

Figure 13 : Observed frequency distribution and normalized Gaussian for data with greater dispersion.

7. FREQUENCY RESPONSE

Figure 14 shows the amplitude response of an actuator. The actuators were found capable of responding to frequencies of up to 66 kHz (Nyquist frequency) without attenuation.

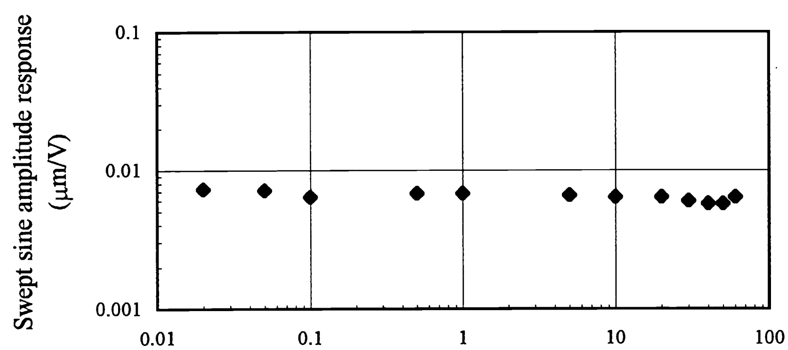

Figure 14 : Amplitude response of a micro-actuator. The sinusoidal drive voltage was 26.3 V (peak to peak) with a 10V DC offset, resulting in 200 μm of maximum deflection.

8. CONCLUSIONS

Because of their relative simplicity in both mechanical and electrical design, the actuators described in this paper are relatively reliable and their behavior is relatively uniform. Statistical performance measurements made on individual actuators have proven that the devices offer repeatability in the 10 nm range. With a usable stroke of more than 0.5 μm and a uniform frequency response up to 66 kHz, these devices show great promise for use as integrated optical array elements.

9. ACKNOWLEDGMENTS

This research is being funded by a three-year contract with DARPA(DABT63-95-C-0065), and was initiated on a Small Grant for Exploratory Research from the National Science Foundation (# DDM9317937). Thanks to the technical personnel at MCNC for their assistance with fabrication-related design issues. Thanks also to Ned Bennett of Zygo Corporation who collaborated on the design of the differential interferometer system. We also thank Adam Maines for software development and Dr. Mark Horenstein for the design and development of control circuitry.

10. REFERENCES

1. R. Krishnamoorthy, T. Bifano, "MEMS arrays for deformable mirrors", *Proceedings of SPIE Microelectronic Structures and Microelectromechanical Devices for Optical Processing and Multimedia Applications*, Vol. 2641, pp. 96-104, Oct. 1995.

2. D.A. Koester, R. Mahadevan, K.W. Markus, "MUMPs Introduction and Design Rules", MCNC Technology Applications Center, 3021 Cornwallis Road, Research Triangle Park, North Carolina, Oct. 1994.

3. J.S.Bendat, A.G.Piersol, *Random Data: Analysis and measurement procedures*, Wiley Interscience, New York, 1986.

4. J.R.Taylor, *An introduction to error analysis : the study of uncertainties in physical measurements*, University Science Books, Mill Valley, California, 1982.